Three Dimensional Reconstruction of Watermelon for Multimedia Traceability System

Junxiang Gao, Xiangyang Xing, and Ruifang Zhai
Hubei Key Laboratory of Agricultural Bioinformatics, College of Informatics, Huazhong Agricultural University, 430070, Wuhan, China
Email: gao200@mail.hzau.edu.cn, 845527667@qq.com

***Abstract*—Traceability system is an important technology for modern agriculture to improve the product quality and increase the brand influence. However, the current traceability system can only provide simply text data so that its effect is very limited. To overcome the shortcoming of text traceability system, we defined the new concept of Multimedia Traceability System (MTS). The multimedia traceability system uses computer technologies to collect, store, process, analyze, transfer and retrieve the data of text, image, graphic, video and voice, also establishes logical relationship among these data and integrates them into an interactive and multidimensional system. We proposed multimedia traceability framework and discussed the involved key technologies. Furthermore, we studied three dimensional reconstruction of fruit used in multimedia traceability system, taken watermelon as an example. We firstly took sequential pictures around watermelon from different angles, performed feature points matching using scale-invariant feature transform algorithm, then generated sparse point cloud and dense point cloud exploiting structure from motion method and multi-view stereo method, respectively. Consequently, texture mapping and model meshing were conducted by means of Poisson surface reconstruction approach. Finally, the accuracy and efficiency of reconstruction were analyzed by experiments.**

***Index Terms*—multimedia traceability system, three dimensional reconstruction, multi-view stereo vision, point cloud, phenotype measurement**

I. Introduction

Traditional agriculture focuses on the increase of output, while modern agricultural industry emphasizes quality improvement, brand influence and the technical level of products. In recent years, the quality traceability system has been paid more and more attention as an effective method to control product quality. Most developed countries have studied and developed the food traceability rules and practical systems [1]-[3]. Many developing countries are also narrowing this gap. Scientists have carried out the researches on the traceability system of agricultural products [4], [5], studied the key elements and technical difficulties of the traceability system, and constructed applicable system with basic functions. These achievements have important significance for subsequent research, but there are still many problems without perfect solutions. One of the serious problems is that the current traceability system can provide manufacturers, product batches, and production of raw materials, but these data are provided with simple text, and unable to show intuitive and comprehensive product information to the consumers. This longstanding technical bottleneck greatly weakens the persuasiveness of the traceability system.

The reason for this problem is that modern multimedia technologies have not been applied in traceability system, therefore we defined the new concept of Multimedia Traceability System (MTS) in this paper, proposed its framework and discussed the involved key technologies. Taken three dimensional reconstruction of watermelon as an example, we gave an application of multimedia traceability system. The reasons for focusing on 3D reconstruction of watermelon are as follows. Firstly, compared with text and ordinary two-dimensional pictures, 3D images can describe the shape, texture and geometric features of the product more truthfully and integrally [6]. Secondly, in the majority of fruit classification assembly-lines, it has become a conventional technology to obtain hundreds of images for a single fruit from multiple angles, and three dimensional reconstruction of the fruit can be realized with the help of the available hardware equipped in assembly-line. At present, 3D reconstruction has been widely applied in many fields, such as architecture, medical treatment, agriculture and so on. Three dimensional reconstruction methods can be divided into three categories: parameter-based method, scanning-based method and image sequence-based method [7], [8]. The parameter-based method is well-studied, but the method is based on prior knowledge, and the reconstruction result is difficult to be consistent with reality, which is only a simple description of the reconstructed object [9]. The scanning-based method can efficiently obtain the 3D spatial data of the reconstructed object [10]. Its disadvantages are the large amount of point cloud data and the high cost of laser scanning equipment, therefore these shortcomings limit the application in agricultural products with lower value. The reconstruction method based on multi-angle sequence images uses ordinary visible light camera to collect the two-dimensional image [11], [12], which is fast and simple, and the cost of the equipment is quite low. The results include the accurate shape, color, texture and geometric parameters of the reconstructed object.

Manuscript received December 15, 2018; revised March 18, 2019.

doi: 10.18178/ijfe.5.1.1-8

In this study, the concept of multimedia traceability system was established and three dimensional reconstruction technologies were studied taking watermelon as an example. To reconstruct 3D watermelon, the pictures were collected around the target, and then the SIFT (scale-invariant feature transform) feature points were detected and matched, and 3D point cloud data of watermelon was obtained using the motion recovery structure method and MVS (multi-view stereo vision) technology, and then the point cloud data was meshed and textured by the point cloud data. Finally, the 3D structure of watermelon was reconstructed and accuracy and efficiency of reconstruction were analyzed by experiments.

II. The Concept of Multimedia Traceability System (MTS)

The breakthrough progress of data processing, transmission and storage in computer science has promoted the development of multimedia technology. The traditional traceability system will get a new promotion if combining modern multimedia technology. On the basis of exploring the limitations of current traceability technology, this paper proposes the concept of multimedia traceability system. The multimedia traceability system uses computer technology to collect, store, process, analyze, transfer and retrieve the data, such as text, image, graphic, video, sound, etc., and establishes the logical relationship between various information so that the collections become an interactive and multi-dimensional system.

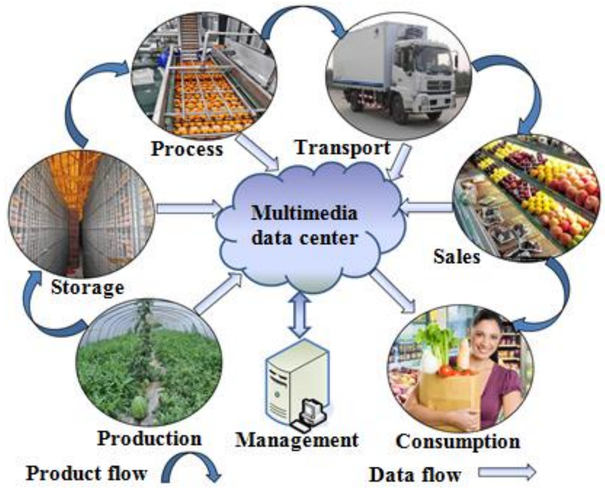

Figure 1. Framework of multimedia traceability system.

The framework of multimedia traceability system is shown in Fig. 1, which describes two kinds of objects: product flow and data flow. In all links of the product, such as production, storage, process, transportation, and sales, the product flows from one link to the next; and each link produces multimedia data that will flow to the data center; of course, the flow of different products may be different for a particular product. But this does not affect the overall rationality of the framework. In multimedia traceability system the flow of products is physical, i.e., the products are delivered from upstream to downstream. While the flow of data is logic, i.e., the multimedia data center may be either centralized or distributed. This is because the multimedia traceability system usually generates large amount of data far more than text system, and the frequent transmission of mass data is not reasonable in technology. What's more, some multimedia data need to be produced and processed in real time in the procedure of production, and it is often not feasible to submit data to a server for centralized processing. In the framework of multimedia traceability system data center is a logical whole.

Multimedia traceability involves the acquisition, processing, analysis and transmission of information in product flow. The information mainly includes the collection of images, video and sound, involves the integrated design of hardware and software, the selection of special chip DSP and the adaption of operating system. The content of multimedia data processing analysis is very rich. Data compression, content recognition, target detection and 3D reconstruction are all important issues in processing and analysis. Because of the huge amount of data, the transmission rate of multimedia data is much higher than text, but it has a higher tolerance to error rate and reliability of the communication channel comparing with traditional text traceability system.

III. Materials and Methods

A. Image Acquisition and Processing

The experimental materials are 3 mature CP8424 watermelons, and the image acquisition device is HUAWEI NOTE8 smart phone. The obtained multi-angle images are in JEPG format and stored in the computer. Using the software platform VisualSFM, Meshlab VS2010 and Netfabb, the three dimensional model of watermelon is reconstructed and the phenotype parameters of watermelon are measured [13]. Image acquisition was carried out under indoor light conditions, and the samples were placed on a bracket with 20×20mm calibrated black-and-white checkerboard. In order to ensure that the top and bottom of the watermelon could be photographed, the pictures were taken from different heights, 300 images for a sample in total (Fig. 2).

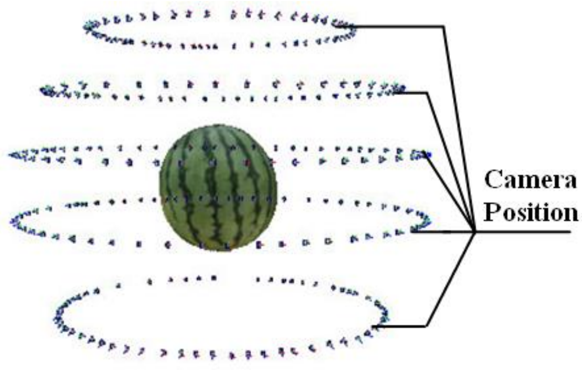

Figure 2. Image acquisition of watermelon. The blue dot around the watermelon. represents the location of the camera.

The flow chart of 3D reconstruction was shown in Fig. 3. The detection and matching of SIFT feature points were carried out by the multi-angle sequence images. Then the sparse three dimensional point cloud of watermelon was calculated by SFM method, and the dense point cloud was generated by MVS technology. Finally, the three dimensional model of watermelon was established by meshing and texture mapping of watermelon data [14], [15].

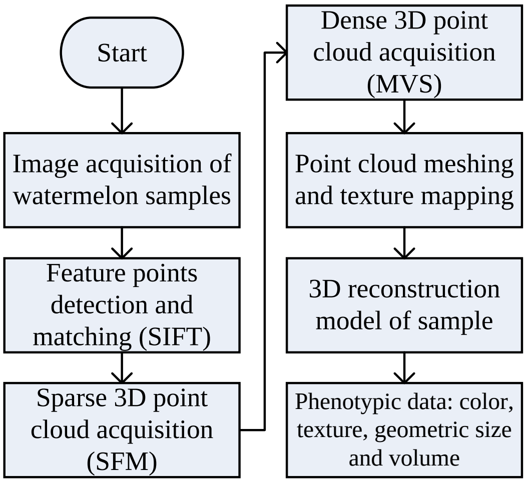

Figure 3. Flow chart of watermelon three dimensional reconstruction

B. *Detection and Matching of Feature Points*

This paper used the scale invariant feature transform (scale-invariant feature transform, SIFT) to detect the key feature points of the image [16]. The SIFT algorithm is invariant to scaling and rotation of the image and illumination changes, also has a certain stability for noise. The algorithm consisted of 4 main steps:

1) Gauss convolution kernel was applied for filter of two-dimensional images, and the scale space of image was obtained. In (1), G was a scale variable two-dimensional Gauss function, and σ was a scale coordinate. Point $I(x, y)$ was the value of image I at coordinates (x, y).

$$\begin{cases} L(x, y, \sigma) = G(x, y, \sigma) * I(x, y) \\ G(x, y, \sigma) = \dfrac{1}{2\pi\sigma^2} \exp\left(-\dfrac{x^2 + y^2}{2\sigma^2} \right) \end{cases} \tag{1}$$

2) Gauss differential scale space was obtained using convolution of the adjacent Gauss difference function, here k is a multiple of two adjacent scale spaces, as shown in (2).

$$\begin{cases} L(x, y, \sigma) = G(x, y, \sigma) * I(x, y) \\ L(x, y, k\sigma) = G(x, y, k\sigma) * I(x, y) \\ D(x, y, \sigma) = L(x, y, k\sigma) - L(x, y, \sigma) \end{cases} \tag{2}$$

3) According to the gradient direction of adjacent pixels, directional assignment was performed for each feature point. The gradient values m and direction θ at the pixels (x, y) were shown in (3), respectively. The scale of L was the scale of each feature point. Gradient histogram was used to calculate the gradient direction corresponding to adjacent pixels, and the histogram peak represented the main direction corresponding to the feature points.

$$\begin{cases} m(x, y) = \sqrt{{L_1}^2 + {L_2}^2} \\ \theta(x, y) = \arctan(L_2 / L_1) \\ L_1 = L(x+1, y) - L(x-1, y) \\ L_2 = L(x, y+1) - L(x, y-1) \end{cases} \tag{3}$$

4) The 8×8 window was taken centered the feature point, and the gradient direction histogram of the 8 directions was calculated for each feature point in the region of 4×4, then the cumulative values of every gradient direction were drawn as a seed point. Each feature point was described with 4×4 total 16 seed points, and 4×4×8=128 dimensional SIFT feature descriptor was generated.

The SIFT feature description operator was a 128 dimensional feature vector. Using the nearest neighbor matching algorithm [16], the ratio of the nearest neighbor distance and the next nearest neighbor distance was used as constraint condition to match the feature of the stereo image, and the random sampling consistency algorithm was used to remove the wrong and unstable matching points to reduce the impact on the sparse point cloud reconstruction in subsequent steps [17]. Fig. 4 showed the feature point detection and matching of two watermelon images from different angles.

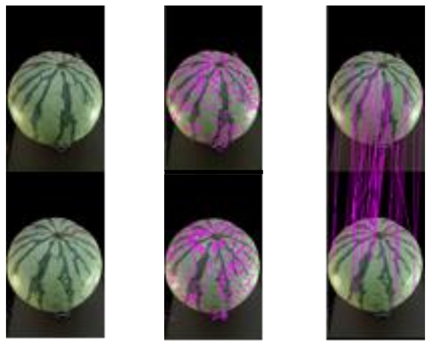

A B C

Figure 4. Feature points detection and matching between two images from different angles. (A) Two watermelon images from different angles. (B) Feature points detection. (C) Feature points matching.

C. *Sparse Point Cloud Reconstruction Based on SFM Technology*

According to the feature point information obtained from the multi-angle sequence images detection and matching, the camera parameters of each image and the three dimensional information corresponding to the two-dimensional matching point were calculated by the method of Structure from Motion (SFM) [18], [19]. This algorithm first calculated essential matrix E based on feature point matching information between two images, and then obtained relative position information containing rotation matrix R and translation vector t by singular value decomposition of the essential matrix E. The relationship between two and three dimensions was established using perspective projection model, and projection formula was obtained in the following. In (4),

K was the parameters of the camera; R and t were rotation matrix and translation vector of the camera, respectively; x was the pixel point in two-dimensional image, and X was 3D point coordinate of x [20].

$$x = K\left[R\,|\,t\right]X \tag{4}$$

D. Dense Point Cloud Reconstruction Based on MVS Technology

To describe the surface information of the reconstructed object more accurately and meticulously, this paper reconstructed dense point cloud using the Clustering views for multi-view stereo and patch-based multi-view stereo algorithm (CMVS/PMVS) [21], [22]. The CMVS algorithm was used to cluster the sequence images. In order to ensure that each sparse point could be accurately reconstructed at least in one subset, the redundant photos were eliminated from the cluster to reduce the amount of dense point cloud and thus improve the computational efficiency.

The seed patch was expanded by PMVS algorithm after clustering. A seed patch p had the following parameters: $c(p)$ was the center of patch p; $n(p)$ was the normal vector to the camera; $R(p)$ was the corresponding reference image; $T(p)$ was the visible image sequence. We projected each image I_i of p into $T(p)$ (the image was divided into $\beta\times\beta$) to identify the corresponding image block C_i (x, y), and each C_i (x, y) was associated with a patch set of Q_i (x, y). For every image C_i (x, y), at least one patch was reconstructed, and new patches were added to the adjacent area until the whole image was covered. Given a patch p, we first determined the set of adjacent image blocks $C(p)$. The initialization conditions for $C(p)$ was as (5).

$$C(p) = \{C_i(x^*, y^*) \,|\, p \in Q_i(x, y), |x - x^*| + |y - y^*| = 1\} \tag{5}$$

Then we removed the image blocks from $C(p)$ according to two constraints. (i) If a patch was already in the image block, there was no need to extend the process. This meant if an image block $C_i(x^*, y^*)\in C(p)$ contained p^*, and p and p^* were adjacent, then removed it from $C(p)$. (ii) If the value of image block was discontinuous, the expansion process was not necessary. The value was continuous or not was determined based on whether the $C_i(x^*, y^*)$ contained a patch with a difference greater than the threshold α, if $C_i(x^*, y^*)$ has generated a slice of the photometric difference less than the threshold value alpha, $C_i(x^*, y^*)$ is deleted from the $C(p)$ without generating a new patch. If $C_i(x^*, y^*)$ has a patch whose difference value was smaller than the threshold, then $C_i(x^*, y^*)$ was deleted from $C(p)$. (iii)We diffused the patches left in the collection $C(p)$ to form new patches and update the information in Q_i (x, y).

E. Meshing and Texture Mapping of 3D Model

Through the previous steps, this paper reconstructed the dense 3D point cloud information. However the result was only a set of three dimensional space points, so the visual result was poor and difficult to measure and analyze. To show the object more realistically, we reconstruct the surface of dense 3D point cloud on the generated surface.

We used the Poisson surface reconstruction (PSR) to mesh 3D models [23]. The algorithm assumed that the sample of point cloud data was s, and each sampling point included two attributes: position p_s and normal vector N_s. The sampling point was on the surface of a model M, and the set of s was denoted as S. By calculating the indicative function χ, the gradient field of χ approximated to the vector domain $\boldsymbol{V}$ defined by the sampling points, i.e., the equation $\min_\chi=\|\nabla\chi-\boldsymbol{V}\|$ was satisfied. Then the problem was transformed into a Poisson equation. The iso-surface of the model was extracted by estimated indicator function χ, and a closed and triangulated estimation was generated. The main steps were in the following.

1) Definition of the gradient domain. The indicative function was a piecewise constant function, thus the computation of the gradient domain would result in infinity in the vector domain of the surface boundary. It was necessary to convolute the indicator function and a smoothing filter to avoid it. Given an entity M with a surface as ∂M, it was assumed that χ_M was an indicator function of M, and $\boldsymbol{N}_{\partial M(p)}$ was the normal vector of inner directional surface of the sampling point p, $\tilde{F}(q)$ was a smooth filter, and $\tilde{F}_p(q)=\tilde{F}(q\text{-}p)$ represented the transformation of the point. Then the gradient domain of the indicative function was equal with the surface normal vector domain as shown in (6).

$$\nabla\left(\chi_M * \tilde{F}\right)(q_0) = \int_{\partial M} \tilde{F}_p(q_0)\,\boldsymbol{N}_{\partial M}(p)\,dp \tag{6}$$

2) Estimation of gradient domain. Estimation of surface integrals was calculated based on normal information provided by directed point set. The point set S divided ∂M into different small patches p_s, and the integral of the small patch set p_s was estimated by the position $s.p$ of the sample point set.

$$\nabla\left(\chi_M * \tilde{F}\right)(q_0) \approx \sum_{s\in S} |p_s| \tilde{F}_{s.p}(q) s.\boldsymbol{N} \equiv \boldsymbol{V}(q) \tag{7}$$

3) Solution of Poisson equation. The least square method $\min_\chi=\|\nabla\chi-\boldsymbol{V}\|$ was used to estimate the optimal solution of $\Delta\chi=\nabla\cdot\boldsymbol{V}$.

4) Extraction of iso-surface. In order to get the reconstructed surface ∂M, we selected an equivalent value of γ and estimate the mean value according to the sampling point $\tilde{\chi}$.

$$\begin{cases} \partial\tilde{M} \equiv \left\{q \in R^3 \,|\, \tilde{\chi}(q) = \gamma\right\} \\ \gamma = \dfrac{1}{|S|}\displaystyle\sum_{s\in S} \tilde{\chi}(s.p) \end{cases} \tag{8}$$

In this paper, an automatic texture mapping method was used to map the pixel value on two-dimensional image bitmap to corresponding vertex of the 3D reconstruction model with the aid of the parameter information obtained in point cloud model reconstruction process [24]. Fig. 5A-5D showed the above 4 steps of the sparse point clouds, dense point clouds, and 3D reconstruction after Poisson's solution and texture mapping.

Figure 5. Three dimensional reconstruction procedures. (A) Sparse point cloud. (B) Dense point cloud. (C) Poisson reconstruction. (D) Texture mapping.

IV. Experimental Results and Analysis

This paper used the above method to reconstruct three dimensional watermelon model, collected multi angle sequence images by visible light camera, detected and matched feature points of the input images by VisualSFM software [25], performed the sparse reconstruction of point cloud and camera calibration, and then completed the dense point cloud reconstruction using CMVS and PMVS. After that, the Meshlab tool was used to carry out meshing and texture mapping in dense point cloud. As the input raw data, sequence images played an important role in the quality of reconstruction models. Images of different numbers and different pixels were tested and analyzed in order to obtain the reasonable image sequence parameters, improve accuracy and efficiency of 3D reconstruction model. Finally, the phenotype parameters of the sample were measured with Netfabb 3D model tool.

A. The Influence of Image Number on Accuracy and Efficiency of Reconstruction

The accuracy and computational efficiency are key indicators for reconstruction of 3D images. To give reasonable image number and pixel resolution are important part of optimizing the three dimensional reconstruction method, on the premise that the model can accurately present the shape and texture of the target, and meet the needs of subsequent analysis and application. In the experiment, we captured 25, 50, 100, 200 and 300 images for each watermelon. Consequently, we performed the 4 steps of the above algorithm, recorded the time consumption, and analyzed the effect of image number on the reconstruction accuracy and efficiency.

Fig. 6 showed the sparse point cloud, dense point cloud, the number of reconstructed points and time consumption of each calculation step when entering different numbers of images. As we could see from Fig. 6A-6C, the dense point cloud could only show the outline of watermelon when there were only 25 images. The outline was clearer for 50 images, but there were still large holes. The dense point cloud had better quality if entering 100 images or more. Fig. 6D shows that the number of sparse points, dense points and meshed surfaces increased in turn for the same number of images. If the images increased from 25 to 300, the number of sparse points, dense points and mesh surfaces increased accordingly, and the number of meshed surfaces increased much more rapidly if the images were more than 100.

Since the number of points and the number of mesh surfaces roughly reflected the reconstruction accuracy, we could get the consistent conclusion from Fig. 6D and Fig. 6B: the accuracy of reconstruction increased gradually with the increase of input images; but a quite good result could be obtained when the number of images reached 100. The effect of the images on the computational efficiency was obtained from Fig. 6E: feature matching, sparse reconstruction and dense reconstruction increased with the number of images. The time of sparse and dense reconstruction had a linear relationship with the images, but the time of feature matching was not linear with the images. If the number of images was more than 100, the time consumption went up sharply. Comprehensive analyzing reconstruction accuracy and time consumption, it showed that if the image sequence was over 100, the quality of reconstruction was little improved, but the time consumption increased rapidly, therefore we used 100 images to reconstruct 3D models.

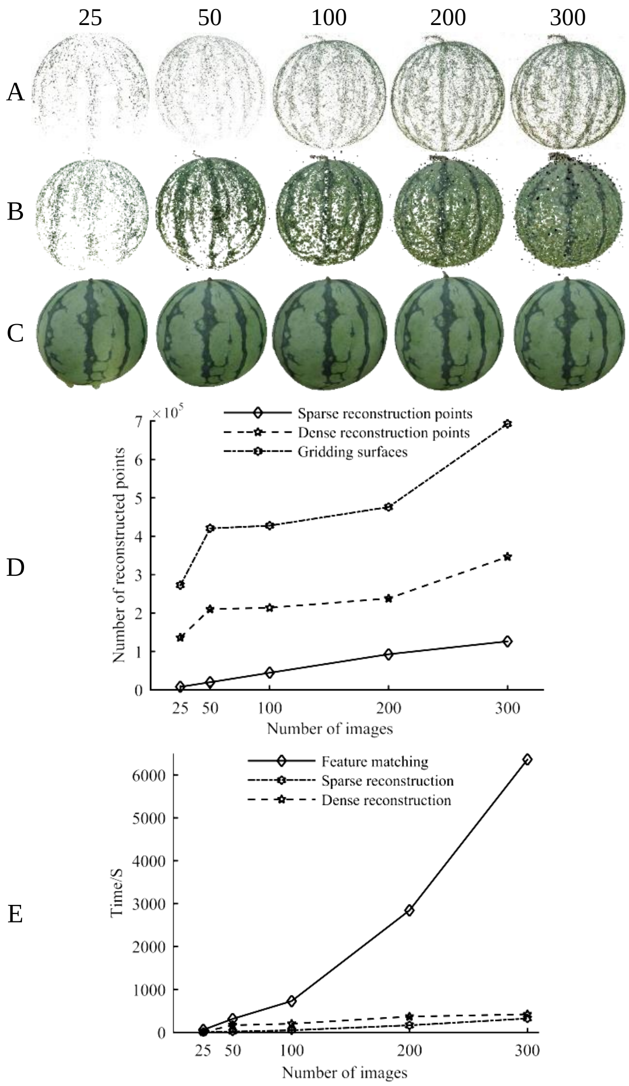

Figure 6. The influence of the image number on the accuracy and efficiency of reconstruction. In figure (A) (B) (C), the number of input images from left to right are 25, 50, 100, 200 and 300. (A) Sparse point cloud. (B) Dense point cloud. (C) Three dimensional reconstruction. (D) The effect of the number of images on the accuracy of reconstruction. (E) The effect of the number of images on the efficiency of reconstruction.

B. *The Influence of Image Resolution on Reconstruction Accuracy and Efficiency*

The resolution of the input image also has a significant effect on the accuracy and efficiency of 3D reconstruction. We captured 100 images with different resolutions including 0.30, 0.50, 1.00, 1.50, 2.00, 4.00 and 6.00 million pixels, respectively, then performed the 4 steps of the algorithm described above, and analyzed the effect of image resolution on reconstruction accuracy and efficiency.

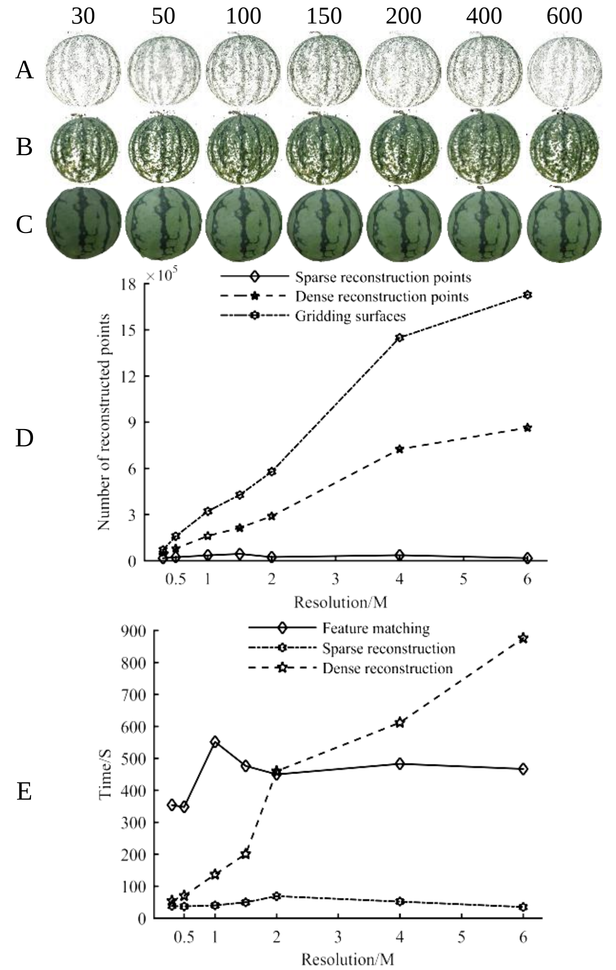

Figure 7. The influence of the image resolution on the accuracy and efficiency of reconstruction. In figure (A) (B) (C), the resolution of input images from left to right are 0.3, 0.5, 1, 1.5, 2, 4, 6 million pixels. (A) Sparse point cloud. (B) Dense point cloud. (C) Three dimensional reconstruction. (D) The effect of the resolution of images on the accuracy of reconstruction. (E) The effect of the resolution of images on the efficiency of reconstruction.

In Fig. 7B, if the resolution is low, such as 0.30 or 0.50 million pixels, dense point cloud had quite large holes. While the resolution exceeded 1.50 million pixels, there was no significant change in quality. In Fig. 7D, if the image resolution increased from 0.50M to 6M pixels, the number of dense points and meshing patches increased with the resolution accordingly. Both of them increased faster if the number of pixels was greater than 2.00M.

Fig. 7E and Fig. 6E showed that the influence of image resolution and image quantity on computing efficiency is quite different. Only time consumption of dense reconstruction increased with the image resolution, while that of sparse reconstruction and feature matching fluctuated in a relatively small range, and it did not have a significant relationship with the image resolution. The experiment indicated that if the resolution was over 1.50M, the quality of reconstruction was little improved, but the time consumption increased rapidly. Therefore, we use 1.50M images to reconstruct 3D models.

C. *Measuring Phenotype Parameters of Watermelon Using 3D Reconstruction*

Three dimensional reconstruction provides information of the shape, texture and color of watermelon for multimedia traceability system. In addition, consumers are concerned about phenotype parameters such as geometric size and volume of the product. According to the conclusion of the previous two experiments, we photographed for 3 watermelons and each had 100 images with 1.50M pixels. As shown in Fig. 8A, the length of the connection between melon top and stalk is denoted as *l*, and the diameter of the cross section is *d*. The result of reconstruction and manual measurement were listed in Table I. The error in the table was calculated on the basis of the measured values. The relative errors were about 1%, which was accurate enough for traceability system.

TABLE I. COMPARISON BETWEEN MANUALLY MEASURED DATA AND RECONSTRUCTED DATA

samples	parameters	manual	3D reconstruction	relative error(/%)
1	*l*/cm	16.20	16.47	1.67
	d/cm	16.92	16.84	-0.47
	volume/cm ³	2596.67	2619.24	0.87
2	*l*/cm	16.80	16.90	0.60
	d/cm	17.06	17.00	-0.35
	volume /cm ³	2635.00	2662.15	1.03
3	*l*/cm	17.60	17.34	-1.48
	d/cm	17.70	17.63	-0.40
	volume /cm ³	3278.33	3221.71	-1.73

Abnormal fruit density often indicates abnormal quality, for example, section-drying. Section-drying is a physiological disease frequently occurring after fruit ripening. The water content of morbidity fruit decreases rapidly, the flavor fades, and the weight of the fruit significantly reduces, which has serious negative effect to the brand selling them to consumers. Our research helps to calculate the fruit density in real time in the production line, and remove the abnormal fruits from the quality traceability system in product classification stage. It is very easy to weigh the fruit automatically in the production line, while to measure the volume accurately is more difficult. Therefore, this paper focused on the latter. A closed model was formed after three dimensional reconstruction, and the volume of watermelon was obtained by calculating the volume of the closed three dimensional model. In order to assure the accuracy of volume calculation using 3D model, we measured the volume of watermelon by drainage method as the exact value and compared them with the former ones. As shown in Fig. 8B, the volume of the water discharged from the bucket was measured using graduated cylinders. The calculated values and the measured values are listed in Table I. It showed that the absolute value of the volume measurement error was about 1%, and the volume of watermelon could be measured accurately through three dimensional reconstruction.

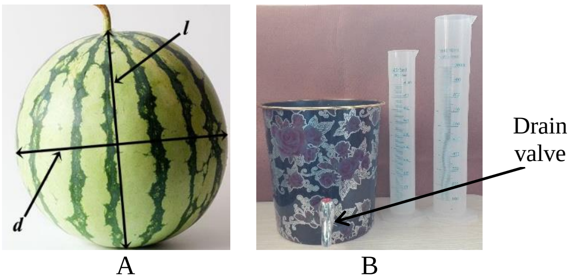

Figure 8. Measuring method of watermelon geometric parameters and volumetric tools. (A) The measurement of the geometric size of watermelon, *l* represents the length of the connection between melon top and stalk, *d* represents the diameter of the cross section. (B) Volumetric tools by drainage method.

V. CONCLUSION

1) In view of the limitation that current traceability system could only provide text information, this paper presented the concept of multimedia traceability system, and discussed its framework, main technical problems and application value. The watermelon was taken as an example to study three dimensional reconstruction of fruit in multimedia traceability system. Acquiring the watermelon image sequence of different angles, the SIFT algorithm is used to detect and match the feature points of the sequence image. The SFM and MVS methods are used to calculate the sparse cloud and dense point cloud, finally the 3D model was accomplished using Poisson surface reconstruction algorithm.

2) We studied the effect of the number of input images on accuracy and efficiency of reconstruction. The results showed that the efficiency of feature matching was much more affected by the number of images than sparse point cloud and dense point cloud. The reconstruction accuracy increased with the number of images, but the quality improvement tended to be slow if the number of images was over 100. Considering above results, one hundred images was obtained with good accuracy and high computational efficiency.

3) We studied the effect of image resolution on accuracy and efficiency. It showed that the time consumption of the feature matching and sparse reconstruction was almost unaffected by image resolution, except for that of dense reconstruction. Image resolution has little influence on reconstruction accuracy. If the resolution was more than 1.50M pixels, the quality of reconstruction was almost no longer improved. Therefore, this study suggested that a high quality watermelon model could be constructed using 1.50M pixel images.

4) Three dimensional reconstruction provided phenotype parameters including shape, color, texture, geometric size and volume. The experiment showed that three dimensional reconstruction could calculate the size and volume accurately. The relative error was about 1%, and the accuracy was enough for multimedia traceability system. In addition, the volume measurement could be used to automatically detect the fruit with abnormal density and remove from the traceability system in the production line.

ACKNOWLEDGMENT

The authors acknowledge financial support from the Fundamental Research Funds for the Central Universities (2013PY087).

REFERENCES

[1] F. Schwägele, "Traceability from a European perspective," *Meat Science*, vol. 71, no. 1, pp. 164-173, 2005.
[2] M. Thompson, G. Sylvia, and M. T. Morrissey, "Seafood traceability in the United States: Current trends, system design, and potential applications," *Comprehensive Reviews in Food Science & Food Safety*, vol. 4, no. 1, pp. 1-7, 2005.
[3] A. Regattieri, M. Gamberi, and R. Manzini, "Traceability of food products: general framework and experimental evidence," *Journal of Food Engineering*, vol. 81, no. 2, pp. 347-356, 2007.
[4] T. Pizzuti and G. Mirabelli, "The global track&trace system for food: general framework and functioning principles," *Journal of Food Engineering*, vol. 1, no. 159, pp. 16-35, 2015.
[5] Y. Dong, B. Ding, G. Zhang, G. Jin, and X. Zhao, "Quality and safety traceability system based on agricultural product supply chain," *Transactions of the Chinese Society of Agricultural Engineering*, vol. 32, no. 1, pp. 280-285, 2016.
[6] C. Zhao, L. Hao, L. Yang, M. Chen, C. Sun, and W. Li, "Design of video record for agricultural products traceability system," *Transactions of the Chinese Society for Agricultural Machinery*, vol. 43, no. 12, pp. 118-122, 2012.
[7] N. Pfeifer and D. Winterhalder, "Modelling of tree cross sections from terrestrial laser scanning data with free-form curves," in *Proc. ISPRS Workshop Laser-Scanners for Forest and Landscape Assessment*, 2004, pp. 76-81.
[8] G. Liu, Y. Si, and J. Feng, "3D reconstruction of agriculture and forestry crops," *Transactions of the Chinese Society for Agricultural Machinery*, vol. 45, no. 6, pp. 38-46, 2014.
[9] J. R. Rosell and R. Sanz, "A review of methods and applications of the geometric characterization of tree crops in agricultural activities," *Computers & Electronics in Agriculture*, vol. 81, no. 4, pp. 124-141, 2012.
[10] P. Raumonen, M. Kaasalainen, M. Åkerblom, S. Kaasalainen, H. Kaartinen, M. Vastaranta, *et al*., "Fast automatic precision tree models from terrestrial laser scanner data," *Remote Sensing*, vol. 5, no. 2, pp. 491-520, 2013.
[11] J. Li, B. Li, F. Liu, and Z. Li, "Generating 3D model of slope eroded gully based on photo reconstruction technique," *Transactions of the Chinese Society of Agricultural Engineering*, vol. 31, no. 1, pp. 125-132, 2015.
[12] J. M. Gilliot, E. Vaudour, and J. Michelin, "Soil surface roughness measurement: a new fully automatic photogrammetric approach applied to agricultural bare fields," *Computers & Electronics in Agriculture*, vol. 134, no. 1, pp. 63-78, 2017.
[13] R. Wróżyński, K. Pyszny, M. Sojka, C. Przybyła, and S. Muratbłażejewska, "Ground volume assessment using 'structure from motion' photogrammetry with a smartphone and a compact camera," *Open Geosciences*, vol. 9, no. 9, pp. 281-294, 2017.
[14] K. Wenzel, M. Rothermel, D. Fritsch, and N. Haala, "Image acquisition and model selection for multi-view stereo," *International Archives of the Photogrammetry, Remote Sensing and Spatial Information Sciences*, pp. 251-258, 2013.
[15] R. Pan and G. Taubin, "Automatic segmentation of point clouds from multi-view reconstruction using graph-cut," *Visual Computer*, vol. 32, no. 5, pp. 601-609, 2016.

[16] D. G. Lowe, "Distinctive Image Features from Scale-Invariant Keypoints," *International Journal of Computer Vision*, vol. 60, no.2, pp. 91-110, 2004.

[17] M. Fischler and R. Bolles, "Random Sampling consensus: A paradigm for model fitting with application to image analysis and automated cartography," *Communications of the ACM*, vol. 24, no. 6, pp. 381-395, 1981.

[18] M. A. Fonstad, J. T. Dietrich, B. C. Courville, J. L. Jensen, and P. E. Carbonneau, "Topographic structure from motion: A new development in photogrammetric measurement," *Earth Surface Processes & Landforms*, vol. 38, no. 4, pp. 421-430, 2013.

[19] Z. Wei, A. Ramon, H. He, and W. Gao, "Accuracy analysis of terrain point cloud acquired by 'structure from motion' using aerial photos," *Seismology & Geology*, vol. 37, no. 2, pp. 636-648, 2015.

[20] J. L. Schönberger, F. Fraundorfer, and J. M. Frahm, "Structure-from-motion for MAV image sequence analysis with photogrammetric applications," *International Archives of the Photogrammetry, Remote Sensing and Spatial Information Sciences*, vol. XL-3, pp. 305-312, 2014.

[21] Y. Furukawa and J. Ponce, "Accurate, dense, and robust multi-view stereopsis," *IEEE Transactions on Pattern Analysis & Machine Intelligence*, vol. 32, no. 8, pp. 1362-1367, 2010.

[22] Y. Furukawa and J. Ponce, "Accurate camera calibration from multi-view stereo and bundle adjustment," *International Journal of Computer Vision*, vol. 84, no. 3, pp. 257-268, 2008.

[23] M. Kazhdan, M. Bolitho, and H. Hoppe, "Poisson surface reconstruction," in *Proc*. *Eurographics Symposium on Geometry Processing*, vol. 32, no. 3, pp. 61-70, 2006.

[24] B. Lévy, S. Petitjean, N. Ray, and J. Maillot, "Least squares conformal maps for automatic texture atlas generation," *ACM Transactions on Graphics*, vol. 21, no. 3, pp. 362-371, 2006.

[25] C. Wu, "Towards linear-time incremental structure from motion," in *Proc. International Conference on 3dtv-Conference*, Seattle, 2013, vol. 8768, no. 2, pp. 127-134.

Junxiang Gao, born in Hebei Province, China in July 1972, received his bachelor's degree in telecommunication at Shanghai Maritime University in 1996 and in 2002 attained his master's degree of electric engineering at Xi'an Jiaotong University. In 2010 he received his PhD degree at Beijing University of Posts and Telecommunications, and started teaching at Huazhong Agricultural University. He is now an associate professor of College of Informatics. Dr. Gao has been engaging in the study of traceability system on food. Recently, he introduced biometric technology into fruit identification of traceability system and proposed a watermelon identification method exploiting texture information of the area around the fruit stalk. Dr. Gao has already published 15 papers and been awarded 2 invention patents.

Xiangyang Xing, born in Hubei Province, China in July 1994. He is currently studying in agricultral inforation engineering in master's program at Huazhong Agricultral University. His research focus is the application of information technology in food safety.

Ruifang Zhai, born in Hubei Province, China in December 1979, received her bachelor's degree in Remote Sensing Technology at Wuhan University in 2001. She attained her Master's and Doctor's degree at same university in 2003 and 2006, respectively. After the postdoctoral study, she started teaching at Huazhong Agricultural University in 2010. She is now an associate professor of College of Informatics. Dr. Zhai has been engaging in the research of 3D reconstruction technology in agricultural application for these years.